

Semi-DRDNet: Semi-supervised Detail-recovery Image Deraining Network via Unpaired Contrastive Learning

Yiyang Shen, Sen Deng, Wenhan Yang, *Senior Member, IEEE*, Mingqiang Wei, *Senior Member, IEEE*, Haoran Xie, *Senior Member, IEEE*, Xiao-Ping Zhang, *Fellow, IEEE*, Jing Qin, Meng Wang, *Fellow, IEEE*

Abstract—The intricacy of rainy image contents often leads cutting-edge deraining models to image degradation including remnant rain, wrongly-removed details, and distorted appearance. Such degradation is further exacerbated when applying the models trained on synthetic data to real-world rainy images. We raise an intriguing question – if leveraging both accessible unpaired clean/rainy yet real-world images and additional detail repair guidance, can improve the generalization ability of a deraining model? To answer it, we propose a semi-supervised detail-recovery image deraining network (termed as Semi-DRDNet). Semi-DRDNet consists of three branches: 1) for removing rain streaks without remnants, we present a *squeeze-and-excitation* (SE)-based rain residual network; 2) for encouraging the lost details to return, we construct a *structure detail context aggregation* (SDCAB)-based detail repair network; to our knowledge, this is the first time; and 3) for bridging the domain gap, we develop a novel contrastive regularization network to learn from unpaired positive (clean) and negative (rainy) yet real-world images. As a semi-supervised learning paradigm, Semi-DRDNet operates smoothly on both synthetic and real-world rainy data in terms of deraining robustness and detail accuracy. Comparisons on four datasets show clear visual and numerical improvements of our Semi-DRDNet over thirteen state-of-the-arts. Code is available at <https://github.com/Dengsgithub/DRD-Net>.

Index Terms—Semi-DRDNet, Detail-recovery Image deraining, Semi-supervised learning, Unpaired contrastive learning

1 INTRODUCTION

Images captured on rainy days inevitably suffer from the noticeable degradation of visual quality. The degradation causes detrimental impacts on outdoor vision-based systems, such as video surveillance, autonomous driving, and monitoring. It is, therefore, indispensable to remove rain in rainy images, which is referred to as image deraining.

The ultimate goal of image deraining is to recover the ground-truth image \mathbf{B} from its observation $\mathbf{O} = \mathbf{B} + \mathbf{R}$ with the rain streaks \mathbf{R} . However, image deraining is an ill-posed yet challenging problem, since 1) \mathbf{B} and \mathbf{R} are both unknown; and 2) \mathbf{B} contains image details similar to \mathbf{R} in scale.

The traditional image deraining methods usually exploit various image priors, such as Gaussian mixture model [5], sparse coding [6], [7] and low-rank representation [8], [9]. However, for this traditional wisdom of image deraining, users have to tweak parameters multiple times to obtain satisfied detection results in

practical scenarios. This inconvenience heavily discounts the efficiency and user experience in medium- and heavy-rain removal.

With the development of deraining networks [10]–[15], the numerical performances on recognized synthetic datasets are already at a high level. Actually, the deraining results cannot be totally expressed only by PSNR or SSIM, since image degradation (e.g., the loss of image details, remnant rain, halo artifacts and/or color distortion) is common to observe in these learning-based methods [16]–[26]. They are prevented from both removing rain streaks completely and preserving image details effectively on real-world rainy images captured from the bad weather. There are mainly three reasons (see the deraining results in Fig. 1):

- (i) Existing the gap between synthetic and real-world rainy images: most existing approaches only use paired synthetic rainy images for training, due to the lack of paired real-world rainy images. Thus, it leads to poor performance on real-world rainy images.
- (ii) Learning the pixel-level correspondence of image pairs via strong supervision: they adopt clean images as positive samples to guide training while neglecting to exploit rainy images as negative samples. The negative samples also provide supervisory information to generate a more discriminative visual mapping.
- (iii) Losing image details during deraining: the magnitude of image details is similar to and even smaller than that of rain streaks; therefore, both are commonly removed simultaneously.

No state-of-the-art methods can serve as a real-world deraining panacea for various applications: they produce deraining results with a trade-off between rain removal and detail preservation.

In this paper, we consider that leveraging both accessible unpaired real-world rainy images and additional detail repair guidance, can improve the generalization ability of a deraining

Y. Shen and M. Wei are with the School of Computer Science and Technology, Nanjing University of Aeronautics and Astronautics, Nanjing, China, and also with the MIT Key Laboratory of Pattern Analysis and Machine Intelligence, Nanjing, China (shenyiyang114@gmail.com; mingqiang.wei@gmail.com).

W. Yang is with the School of EEE, Nanyang Technological University, Singapore. (wenhan.yang@ntu.edu.sg).

H. Xie is with the Department of Computing and Decision Sciences, Lingnan University, Hong Kong SAR, China (hrxie2@gmail.com).

S. Deng and J. Qin are with the School of Nursing, The Hong Kong Polytechnic University, Hong Kong SAR, China (sendeng@nuaa.edu.cn; harry.qin@polyu.edu.hk).

X.-P. Zhang is with the Department of Electrical, Computer and Biomedical Engineering, Ryerson University, Toronto, Canada (xzhang@ee.ryerson.ca).

M. Wang is with the School of Computer Science and Information Engineering, Hefei University of Technology, Hefei, China (eric.mengwang@gmail.com).



Fig. 1. Real-world image deraining in our established real-world dataset, called Real200. Although challenging to cope with real-world rainy images, Semi-DRDNet not only safeguards our result from rain remnants, but also provides the rain-affected areas with abundant real details, which is largely different from its competitors including our conference version, i.e., DRD-Net [4].

model. Therefore, beyond the existing image deraining wisdom, we propose a semi-supervised detail-recovery image deraining network (Semi-DRDNet). Semi-DRDNet can leverage unpaired clean/rainy yet real-world images to improve the generalization ability while recovering image details clearly. The main contribution can be concluded as follows:

- We propose a semi-supervised detail-recovery image deraining network. Our semi-supervised learning paradigm smoothly bridges the domain gap between synthetic and real-world rainy images.
- Semi-DRDNet consists of three branches. The first two branches are parallel and trained on paired synthetic data. The third branch is connected with the first two branches in a cascaded way and provides additional supervision information for unsupervised training.
- For the first branch, we propose a squeeze-and-excitation (SE)-based rain residual network (RRN) to exploit spatial contextual information for complete rain removal.
- For the second branch, we propose a detail repair network (DRN) to encourage the lost details to return to the image after deraining by the rain residual network. To our knowledge, this is the first time.

- To avoid pixel-correspondence paired training data, we propose an unpaired contrastive regularization network (UCR). This is our third branch which trains on unpaired positive/negative samples.
- Semi-DRDNet outperforms thirteen methods both quantitatively and qualitatively on four datasets.

Difference from our conference paper: This work covers and extends our conference version DRD-Net [4] from the following aspects: (i) We generalize DRD-Net to Semi-DRDNet, a new semi-supervised image deraining paradigm to bridge the domain gap between synthetic and real-world rainy data. Thus, our previous DRD-Net can be seen as a simplified version of Semi-DRDNet. (ii) We propose an unpaired contrastive regularization network, which leverages unpaired positives (clean images) and negatives (real rainy images) to build a more generalized and discriminative semi-supervised deraining paradigm. (iii) Both the proposed detail recovery network and unpaired contrastive regularization network are plug-in modules and can be incorporated into existing deraining methods, e.g., [3], [27], to boost their performance. (iv) We build a new real-world rainy dataset, called Real200, which contains 400 real-world rainy images (200 images for training and 200 images for testing) from [16], [28]–[31] and

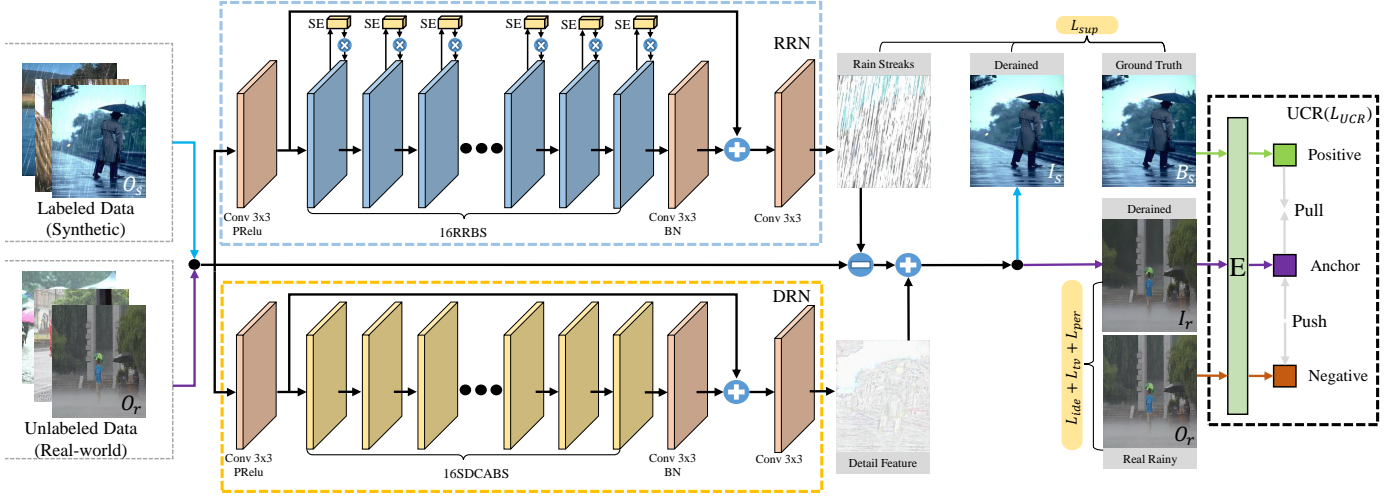


Fig. 2. Pipeline of our Semi-DRDNet. Semi-DRDNet consists of three branches, i.e., the rain removal network (RRN), the detail repair network (DRN) and the unpaired contrastive regularization network (UCR). The first two branches are parallel and then connected to the third branch in a cascaded way. Thus, Semi-DRDNet can remove rain and recover image details, and then be transferred to handle real-world data without labels. In detail, the first network, which combines the squeeze-and-excitation (SE) operation with residual blocks to make full advantage of spatial contextual information, aims at removing rain streaks from the rainy images. The second network, which integrates the structure detail context aggregation block (SDCAB) to aggregate context feature information from a large reception field, seeks to recover the lost details to the derained images. The third network, which utilizes contrastive learning to obtain the information of real-world rainy images and clean images as negative and positive samples, aims to encourage the derained images and the clean images to pull together in the embedding space while pushing them away from the rainy images. Note that O_s , I_s and B_s represent the rainy image, the derained image, and the clean image of synthetic data with labels, respectively. O_r and I_r represent the rainy image and the derained image of real-world data without the corresponding clean images as labels, respectively.

Google search with “real rainy image”. Thus, we conduct more experiments on the synthetic and real-world datasets to verify the superior performance as compared to existing methods. (v) Our results show clear improvements over its previous version, i.e., DRD-Net [4] on real-world rainy images.

2 MOTIVATIONS

Image degradation, such as remnant rain, wrongly-removed details, and distorted appearance, will happen when applying cutting-edge deraining models on rainy images, due to the intricacy of rainy image contents. Such degradation is further exacerbated if applying the models trained on synthetic data to real-world rainy images. At the top level, it is natural to 1) train two parallel networks on paired synthetic clean/rainy images, which are responsible for rain removal and image detail recovery; and 2) train an additional network on unpaired clean/rainy yet real-world images. Such a learning paradigm (two parallel networks via supervision + one cascaded network via unsupervised constraints) will bridge the domain gap between synthetic and real-world rainy images. Therefore, given any real-world rainy image as input, the network is expected to output a derained result without both remnant rain and the loss of image details.

Motivation 1. The current wisdom of image deraining usually leads to the loss of image details, since rain streaks and image details are both of high frequency in nature and they inevitably share similar geometrical properties. We find that most of the existing image deraining networks pay little attention to recovering image details, once they are lost during deraining.

An effective image deraining network should involve the estimation of two components: rain streaks and image details. However, learning both components simultaneously by a single network is somewhat challenging. This motivates us to leverage an additional network, i.e., the detail repair network (DRN), to facilitate the single deraining networks for image detail recovery.

Motivation 2. Unfortunately, the aforementioned two-branch network (one for rain removal, the other for detail recovery) trained on synthetic rainy datasets still operates poorly on real-world rainy images, due to the domain shift problem.

As one may know, it is very easy to collect real-world rain-free and rainy images. If denoting the real-world rain-free images as positive samples, and the real-world rainy images as negative samples, we can potentially learn to pull the derained images together with the positives and push them apart from negatives in a representation space [32]–[35]. However, these real-world rain-free and rainy images are unpaired. Inspired by the recent work of image dehazing [36] and low-light image enhancement [37], we explore an unpaired contrastive regularization network (UCR), which is trained on the unpaired positives and negatives, thus enhancing the real-world image deraining performance.

3 SEMI-DRDNET

We propose a semi-supervised detail-recovery image deraining network (Semi-DRDNet) as shown in Fig. 2. For both real-world rain removal and detail recovery of single images, different from existing solutions, Semi-DRDNet consists of three branches. First, we introduce a rain residual network (RRN) to train a function that maps the rainy images to their rain streaks. Therefore, we can obtain the preliminary derained images by separating the rain streaks from the rainy images. Second, different from other methods which try to decompose a single rainy image into a background layer and a rain streak layer, we present an additional detail repair network (DRN) to get back the lost details. Third, we present a novel unpaired contrastive regularization network (UCR) to improve the quality of real-world derained images.

3.1 Rain Residual Network

Residual learning is a powerful tool for image restoration tasks like denoising and deraining [18], [38]. Since rain streaks are

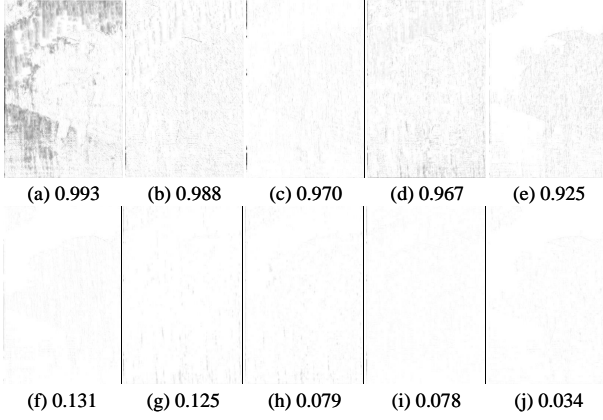


Fig. 3. Feature maps with different weights. The images in (a)-(e) denote the top five high weighted feature maps, and the images in (f)-(j) denote the top five low weighted feature maps. Note that we have inverted these images for better visualization.

sparser than the rain-free background scene [18], we develop a rain residual network (RRN) to map the rainy image to rain streaks.

Our rain residual network utilizes the Squeeze-and-Excitation (SE) [39] operation (see the top part of Fig. 2). Considering that the skip-connections can provide long-range information compensation and enable the residual learning [40], we combine SE with the residual block in our rain residual network, which is different from Fig. 5(c) used in RESCAN [18]. The rain residual network includes 3 convolution layers and 16 rain residual blocks. The first layer can be interpreted as an encoder, which is used to transform the rainy image into the feature maps, and the last two layers are used to recover the RGB channels from feature maps.

Mathematically, the rain residual block is formulated as

$$RRB = SE(Res(\mathbf{X}_0)), \quad (1)$$

where RRB is the output of the rain residual block, $SE(\cdot)$ and $Res(\cdot)$ denote the SE operation and the residual block as shown in Fig. 5(d) respectively, and \mathbf{X}_0 is the input signal.

Spatial contextual information is effective in image deraining [18], [41]. Nevertheless, the different feature channels in the same layer are independent and have few correlations during the previous convolution operation. A main difference from the common residual block is that we combine SE into the residual block. Since SE models a correlation between different feature channels, we can intensify the feature channel which has more context information by giving a larger weight. Conversely, the feature channels that have less spatial contextual information will just receive a small weight. All the weights of different channels are learned by the rain residual network automatically during the training steps. To obtain insight into the correlation between the SE weight and the content of layers, we visualize the feature maps with different weights as shown in Fig. 3. It is clear that the feature maps with more spatial contextual information have received a higher weight as expected.

3.2 Detail Repair Network

Image deraining leads to image degradation in nature. We can train an additional detail-recovery network (DRN) that makes the detail-lost images reversible to their artifact-free status. Inspired by [42], we design our detail repair network based on the structure detail context aggregation block (SDCAB). The difference from

[42] is that we adopt SDCAB into the whole network flow to make full use of multi-scale features, while [42] only applies the multi-scale dilated blocks in the first layer to extract image features. We validate that this modification benefits our detail recovery network. Specifically, SDCAB consists of different scales of dilated convolutions and 1×1 convolutions as shown in Fig. 5(d). Since a large receptive field is very helpful to acquire much contextual information [18], we present 3 dilated convolutions whose dilation scales are 1, 3 and 5 in SDCAB, respectively. Then, in order to extract the most important features, we concatenate the output of dilated convolutions and utilize the 1×1 convolution to reduce the feature dimensions. For reducing the complexity in training, the residual network is also introduced into SDCAB.

As shown in Fig. 5(d), the dilated convolution concatenation layer (DCCL) can be expressed as

$$DCCL = Conv_{1 \times 1}(Cat[Conv_{3 \times 3, d_1}(X), Conv_{3 \times 3, d_3}(X), Conv_{3 \times 3, d_5}(X)]), \quad (2)$$

where $Conv_{x \times x, d_y}$ denotes the dilated convolutions with the kernel size of $x \times x$, and the dilation scale is y . $Cat(\cdot)$ is a concatenation operation and X is the input feature.

Mathematically, SDCAB can be formulated as

$$SDCAB = Add[X_{input}, BN(DCCL_2)], \quad (3)$$

where $DCCL_2$ is described as

$$DCCL_2 = PRelu(BN(DCCL_1(X_{input}))). \quad (4)$$

A large receptive field plays an important role in obtaining more information. With a larger receptive field, we obtain more context information, which is helpful to find back the lost details. One knows from Fig. 4 that, Semi-DRDNet has found back the details that were lost by filtering the rainy image to obtain the final derained image X . We have provided more experimental results on three datasets to compare the performance of image deraining with and without the additional detail repair network (DRN) in Table 2: our Semi-DRDNet outperforms other network architectures thanks to its capability to find back the lost details.

Relationship between our SDCAB and MSARR in [42].

The similarity between the proposed SDCAB and multi-scale aggregated recurrent ResNet (MSARR) in [42] is the use of dilated convolution, which is not new, while the differences lie in several aspects: (i) In [42], the dilated convolution is applied only once to extract features from the original image. In contrast, our network employs several SDCABs, and one SDCAB is composed of several dilated convolution concatenation layers (DCCLs). Such a structure further enlarges the receptive field, which benefits a lot for capturing non-local correlations among details. (ii) In [42], the features extracted by parallel dilated convolution layers are simply added together, while those extracted by DCCL are concatenated and combined with automatically adjusted weights. This benefits the utilization of features from different dilated scales and the localization of image details. (iii) The skip connection is combined with DCCL to construct SDCAB, which not only helps reuse the previous features and explore new ones but also prevents this deep structure from gradient vanishing.

Parallel vs Cascaded: A cascaded network also facilitates the detail recovery, but we avoid adopting it for two reasons: First, a parallel design allows synchronous processing of the two branches and thus is more efficient. Second, the original input provides the detail recovery branch with more detailed features.

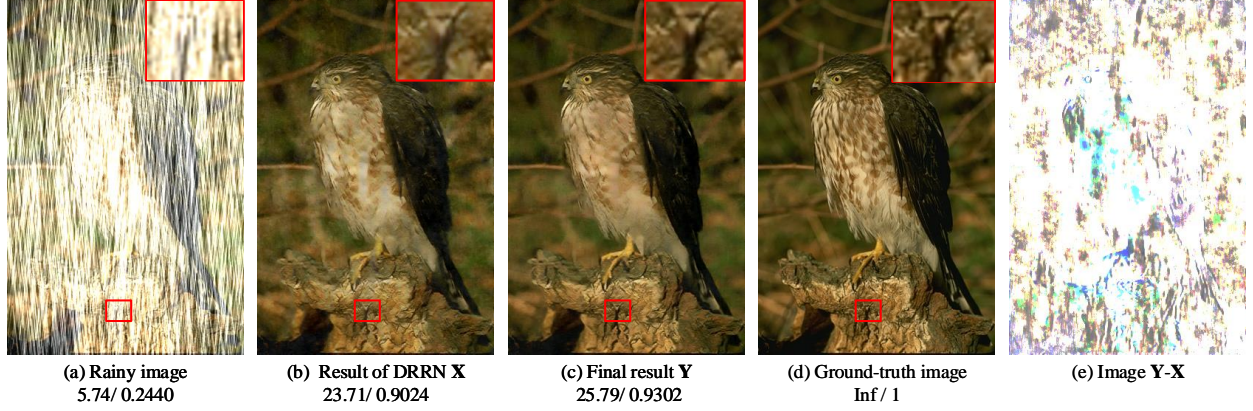


Fig. 4. Image deraining results tested on the dataset of Rain200L. From (a)-(e): (a) the input rainy image, (b) the result X by only using the rain residual network (i.e., without the detail repair network), (c) the result Y by the Semi-DRDNet, (d) the ground-truth image, and (e) the image of $Y-X$ (note: we have inverted the image $Y-X$ for better visualization).

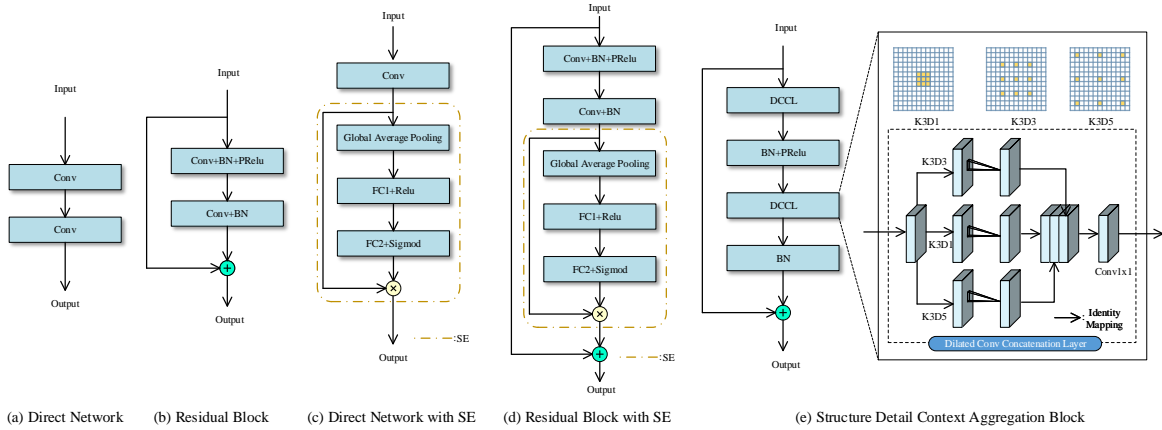


Fig. 5. Different convolution styles. From (a)-(d): (a) direct network, (b) residual block, (c) direct network with SE [18], (d) rain residual block with SE used in our rain residual network, and (e) structure detail context aggregation block used in our detail repair network.

3.3 Unpaired Contrastive Regularization Network

To bridge the domain gap between synthetic and real-world rainy images, we leverage an unpaired contrastive regularization network (UCR) to improve the performance and the generalization capability in real applications.

The goal of UCR is to learn a representation to pull “positive” pairs in the embedding space and push apart the representation between “negative” pairs. We should consider the following aspects: to build the pairs of “positive” and “negative” samples, and to find the suitable latent feature space of pairs to train the network. Thus, we first choose the real-world derained image I_r , the clean image B_r , and the real-world rainy image O_r as the anchor, positive sample, and negative sample, respectively. Then, we select a pre-trained VGG-16 to extract the common intermediate feature for the latent feature space. The unpaired contrastive loss is formulated as

$$L_{UCR} = \sum_{i=1}^n \omega_i \cdot \frac{\|\varphi_i(B_r) - \varphi_i(I_r)\|_2^2}{\|\varphi_i(O_r) - \varphi_i(I_r)\|_2^2}, \quad (5)$$

where $\varphi_i(\cdot)$, $i = 1, 2, \dots, n$ refer to extracting the i -th hidden features from the pre-trained VGG-16 network. Here we choose the 2-nd, 3-rd, and 5-th max-pooling layers. ω_i are weight coefficients, and we set $\omega_1 = 0.2$, $\omega_2 = 0.5$, and $\omega_3 = 1$.

The latest image dehazing method [36] trains a contrastive network on the paired positive (clean) and negative (hazy) samples. However, pairs of real-world rainy images and clean images are intractable to obtain. Thus, we explore an effective unpaired contrastive network for training. Recently, [43] observes that contrastive learning for visual representation can gain significantly from randomness. Thus, we decide to randomly collect the clean images from labeled synthetic datasets as positive samples, which are unpaired with the negative samples (real-world rainy images), and captured under different real-world domains. Through extensive experiments on different datasets, we show that UCR can improve the deraining quality, especially with heavy rain.

3.4 Comprehensive Loss Function

The comprehensive loss function can be formulated as

$$L_{total} = L_{sup} + \lambda_{unsup} L_{unsup}, \quad (6)$$

where λ_{unsup} is a pre-defined weight that controls the contribution from L_{sup} and L_{unsup} .

Supervised training phase: In this phase, we use the labeled synthetic data to learn the network parameters. Specifically, we minimize the supervised loss function as

$$L_{sup} = L_d + \lambda_r L_r, \quad (7)$$

where L_r and L_d are the rain residual loss and the detail repair loss, respectively. They are defined as

$$L_r = \|f(\mathbf{O}_s) - \hat{\mathbf{R}}\|_1, \quad (8)$$

$$L_d = \|(\mathbf{I}_s + g(\mathbf{O}_s) - \mathbf{B}_s)\|_1, \quad (9)$$

where $f(\cdot)$ and $g(\cdot)$ are the functions of RRN and DRN respectively, \mathbf{O}_s is the labeled rainy image, $\hat{\mathbf{R}}$ is the ground-truth rain streak layer obtained by subtracting the ground truth \mathbf{B}_s from the rainy image \mathbf{O}_s , and \mathbf{I}_s is the preliminary derained image obtained by subtracting the generated rain streaks R from \mathbf{O}_s .

Unsupervised training phase: We leverage the unlabeled real-world data to improve the generalization performance. Specifically, we minimize the unsupervised loss function as

$$L_{unsup} = \lambda_{tv}L_{tv} + \lambda_{ide}L_{ide} + \lambda_{per}L_{per} + \lambda_{ucr}L_{UCR}, \quad (10)$$

where L_{tv} , L_{ide} , L_{per} and L_{UCR} are the TV loss, identity loss, perceptual loss and unpaired contrastive loss, respectively.

To preserve both structures and details of input images, we use the total variation (TV) loss [44] on the derained image I_r to constrain the spatial smoothness of a background scene as

$$L_{tv} = \|\nabla_x(I_r) + \nabla_y(I_r)\|_1, \quad (11)$$

where ∇_x and ∇_y represent the horizontal and vertical differential operation matrices, respectively.

To improve the quality of the final generated image, we adopt the identity loss [45] to make the real-world derained images consistent with the real-world rainy images O_r as

$$L_{ide} = E_{I_r \sim P_{data(O_r)}}[\|I_r - O_r\|_1]. \quad (12)$$

The identity loss can minimize the structural difference between the input and generated images, thus generating both rain-free and perceptually more pleasing results.

Inspired by [46], the extracted features from pre-trained models contain rich semantic information, and the distances can act as the perceptual similarity measure, thus, we adopt a perceptual loss [46] to calculate perceptual similarity as

$$L_{per} = \|VGG(I_r) - VGG(O_r)\|_2^2, \quad (13)$$

where $VGG(\cdot)$ denotes the feature maps extracted from the 2nd and 5th pooling layers within VGG-16 pre-trained on ImageNet.

4 EXPERIMENT AND DISCUSSIONS

4.1 Dataset

Synthetic Datasets: For labeled synthetic images, we evaluate the performance of the proposed method on the commonly tested benchmark datasets: (1) Rain200L [47] consists of 1800 training images and 200 test images with only one type of rain streaks; (2) Rain200H [47] also contains 1800 training images and 200 test images, but with five streak directions; (3) Rain800 [16] contains 700 training images and 100 testing images, which are synthesized following the guidelines in [47].

Real-world Datasets: For unlabeled real-world images, we build a new real-world rainy dataset called Real200, which contains 400 real-world rainy images (200 training images and 200 testing images) from [16], [28]–[31] and Google search with “real rainy image”. Since Semi-DRDNet and some compared approaches are trained in a semi-supervised manner, following the protocols of [3], [48], [49], we train them on three

synthetic datasets (Rain200H, Rain200L, and Rain800) as labeled data and Real200 as unlabeled data, which are denoted by $\&$, such as Rain200H $\&$ Real200, Rain200L $\&$ Real200, and Rain800 $\&$ Real200.

4.2 Training Details

We implement Semi-DRDNet using Pytorch 1.6 on a system with 11th Gen Intel(R) Core(TM) i7-11700F CPU and Nvidia GeForce RTX 3090 GPU. During training, we set the depth of our network as 35, and utilize the non-linear activation PReLU [50]. For optimizing our network, we employ the Adam optimizer [51] with the first momentum value of 0.9, the second momentum value of 0.999, and a weight decay of zero. We initialize the learning rate as $6e^{-4}$. All training images are cropped into 256×256 patches with a batch size of 4. We set λ_{unsup} , λ_r , λ_{tv} , λ_{ide} , λ_{per} and λ_{ucr} to be 0.5, 0.1, 0.1, 0.5, 0.5 and 0.5, respectively.

4.3 Comparison with the State-of-the-Arts

Baselines: We compare Semi-DRDNet with thirteen state-of-the-art deraining methods, including two prior-based methods, i.e., GMM [5], and DSC [52]; eight supervised deraining methods, i.e., DDN [10], RESCAN [18], DAF-Net [53], SPA-Net [54], PReNet [55], MSPFN [2], DRD-Net [4] and MPRNet [1]; three semi-supervised deraining methods, i.e., SIRR [28], Syn2Real [3] and JRGR [27]. For the evaluations on synthetic and real-world images, all the supervised methods are directly trained on Rain200H, Rain200L, Rain800, and the semi-supervised ones are trained on Rain200H $\&$ Real200, Rain200L $\&$ Real200 and Rain800 $\&$ Real200. In the quantitative evaluation, Peak Signal-to-Noise Ratio (PSNR) and Structure Similarity Index (SSIM) are used as the comparison criteria. More details of PSNR and SSIM can be seen in [56]. Usually, a larger PSNR or SSIM presents a better result.

Comparisons on the synthetic test sets: Our method clearly outperforms all the deraining methods in terms of both PSNR and SSIM, as shown in Table 1. Especially, the proposed method obtains more than 0.5 dB, 0.36 dB, and 0.64 dB PSNR gains on the test sets of Rain200L, Rain200H, and Rain800, compared with the supervised MPRNet [1]. Besides, the PSNR of our Semi-DRDNet gains over the semi-supervised Syn2Real [3] more than 3.43 dB, 2.92 dB, and 2.08 dB on Rain200L, Rain200H, and Rain800. Such large gains demonstrate the superiority of the proposed semi-supervised paradigm on synthesized rain images. Furthermore, compared to DRD-Net [4] (our conference version), Semi-DRDNet can take advantage of unlabeled real-world data to improve the accuracy of image deraining, and obtain 0.67 dB, 0.5 dB, and 0.38 dB PSNR gains on Rain200L, Rain200H, and Rain800 respectively. We also show the visual results of different methods in Fig. 6 and Fig. 7. It can be observed that Semi-DRDNet not only successfully removes the majority of rain streaks, but also effectively avoids image degradation caused by deraining, and better preserves texture details. Although most approaches can remove the rain streaks from the rainy image, the halo artifacts and color distortion have appeared after deraining.

Comparisons on real-world rainy images: We also evaluate the proposed method on the real-world testing set of Real200 as shown in Figs. 8-14. Figs. 8-9 show the results on real-world rainy images that only contain rain streaks. It is illustrated that, the proposed method can effectively remove most raindrops (Fig. 8) and large rain streaks (Fig. 9), and also better preserve texture details (Fig. 8). Figs. 10-12 show the heavy rain scenes with

TABLE 1

Quantitative experiments evaluated on the testing sets of Rain200L, Rain200H and Rain800. All the supervised methods are directly trained on Rain200H, Rain200L, Rain800, and the semi-supervised ones are trained on Rain200H&Real200, Rain200L&Real200 and Rain800&Real200.

Dataset	Rain200L		Rain200H		Rain800	
	PSNR	SSIM	PSNR	SSIM	PSNR	SSIM
GMM [5]	27.16	0.8982	13.04	0.4673	24.04	0.8675
DSC [52]	25.68	0.8751	13.17	0.4272	20.95	0.7530
DDN [10]	33.01	0.9692	24.64	0.8489	24.68	0.8739
RESCAN [18]	36.39	0.9767	26.60	0.8974	24.09	0.8410
DAF-Net [53]	32.07	0.9641	24.65	0.8607	25.27	0.8895
SPA-Net [54]	31.59	0.9652	23.04	0.8522	22.41	0.8382
PReNet [55]	36.76	0.9796	28.08	0.8871	26.61	0.9015
MSPFN [2]	32.98	0.9693	27.38	0.8690	25.59	0.8882
MPRNet [1]	37.32	0.9810	28.32	0.9168	26.10	0.8967
SIRR [28]	35.46	0.9726	26.89	0.8463	24.36	0.8698
Syn2Real [3]	34.39	0.9657	25.76	0.8370	24.24	0.8667
JRGR [27]	31.98	0.9669	23.46	0.8449	22.16	0.8228
DRD-Net [4]	37.15	0.9873	28.16	0.9201	26.32	0.9018
Semi-DRDNet	37.82	0.9884	28.68	0.9236	26.74	0.9042

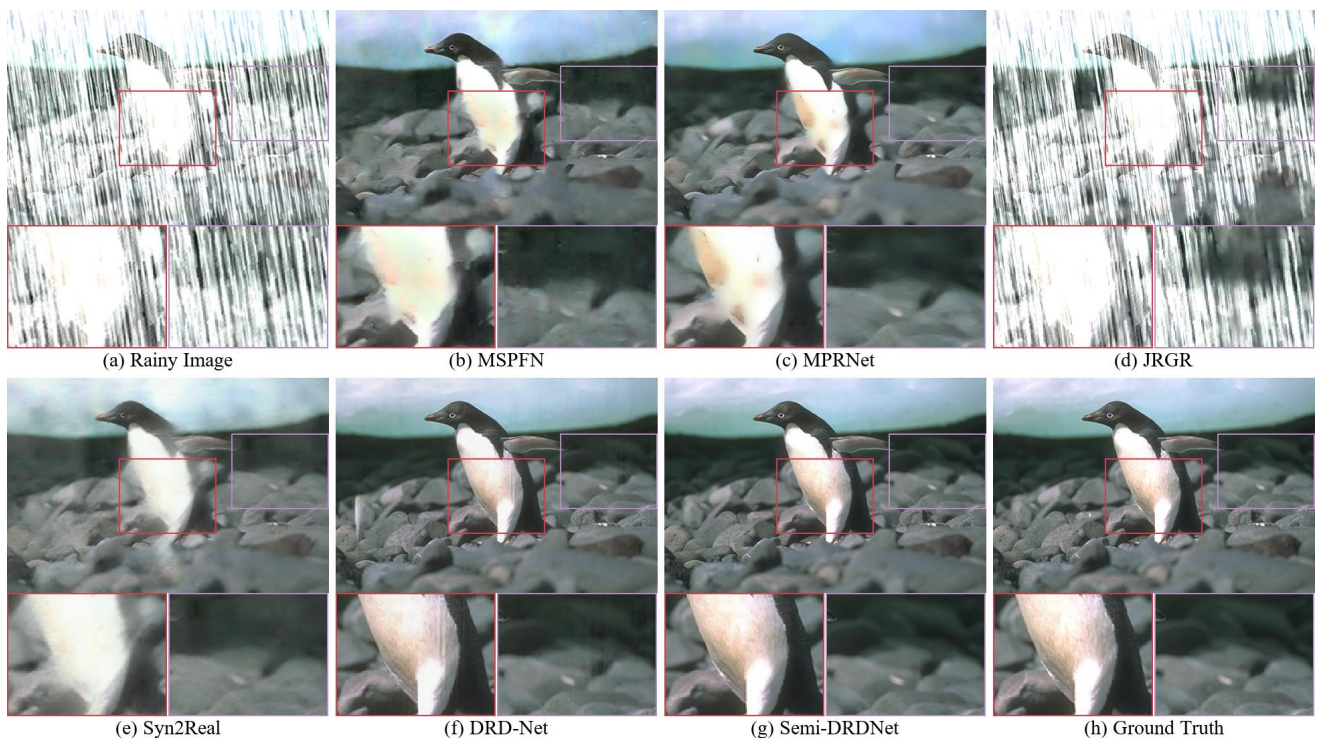


Fig. 6. Image deraining results tested in Rain200H. From (a)-(h): (a) the rainy image, the deraining results of (b) MSPFN [2], (c) MPRNet [1], (d) JRGR [27], (e) Syn2Real [3], (f) our DRD-Net [4], (g) our Semi-DRDNet and (h) the ground truth, respectively.

rain streaks and rainy haze, our method still restores the best results. Note that other methods fail to remove the rain streaks in heavy rain images. Comparatively, our method is more successful to handle heavy rain streaks. Further, Figs. 13-14 represent the nighttime rainy images, without global uniform atmospheric light, the deraining results of most approaches become darker and some details turn invisible, while our Semi-DRDNet still achieves relatively better deraining results. Compared to DRD-Net [4], our Semi-DRDNet achieves limited improvement on the synthetic rainy images, but achieves superior deraining performance on various types of real-world rainy images. Figs. 8-14 show our Semi-

DRDNet can effectively remove the rain streaks while preserving their details, such significant improvement demonstrate that the semi-supervised learning paradigm and the unpaired contrastive regularization network significantly boost the performance on real-world rain images.

User study on real-world rainy images: Evaluation on real-world data that lacks the ground truths is commonly difficult and subjective. We conduct a user study for subjective assessment: (1) To ensure fairness, we randomly choose 50 images covering different scene types from the test set of Real200. (2) We recruit 100 volunteers to rank each deraining result with the score from 1

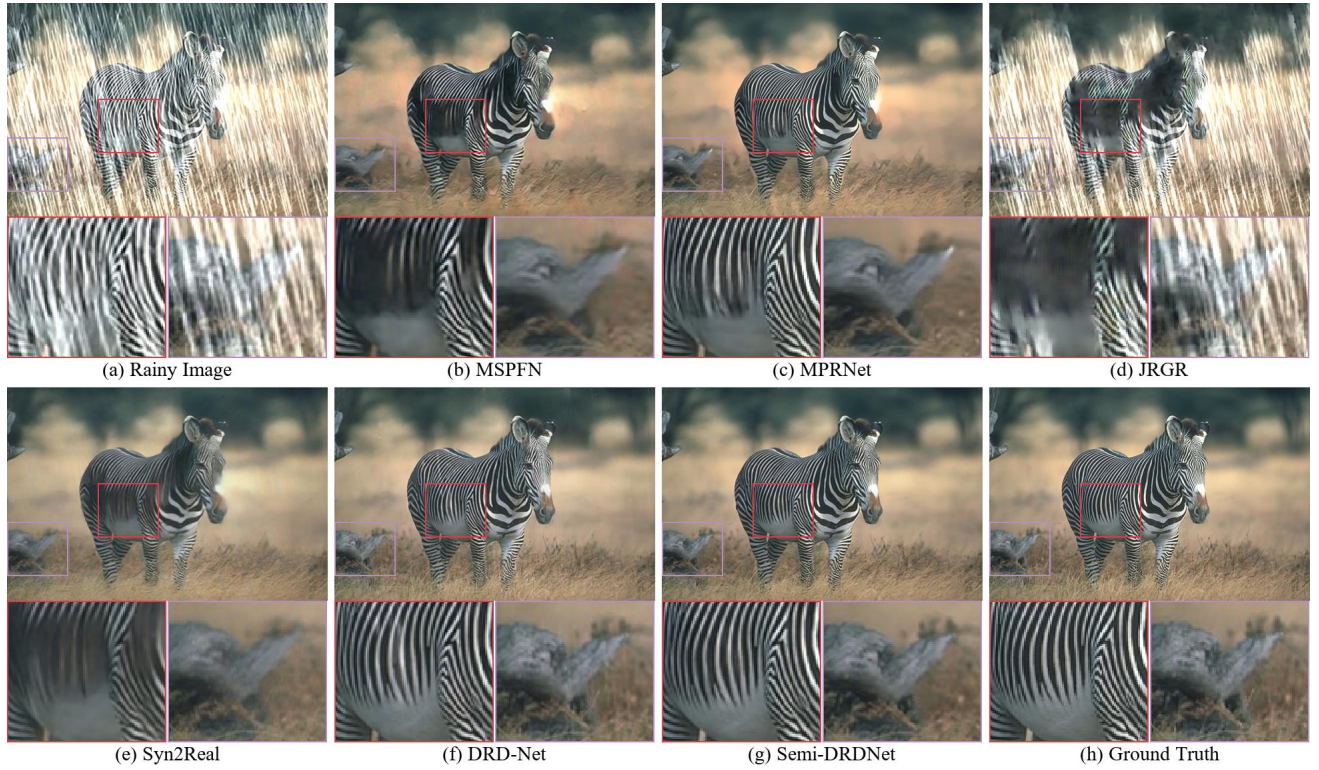


Fig. 7. Image deraining results tested in Rain200H. From (a)-(h): (a) the rainy image, the deraining results of (b) MSPFN [2], (c) MPRNet [1], (d) JRGR [27], (e) Syn2Real [3], (f) our DRD-Net [4], (g) our Semi-DRDNet and (h) the ground truth, respectively.

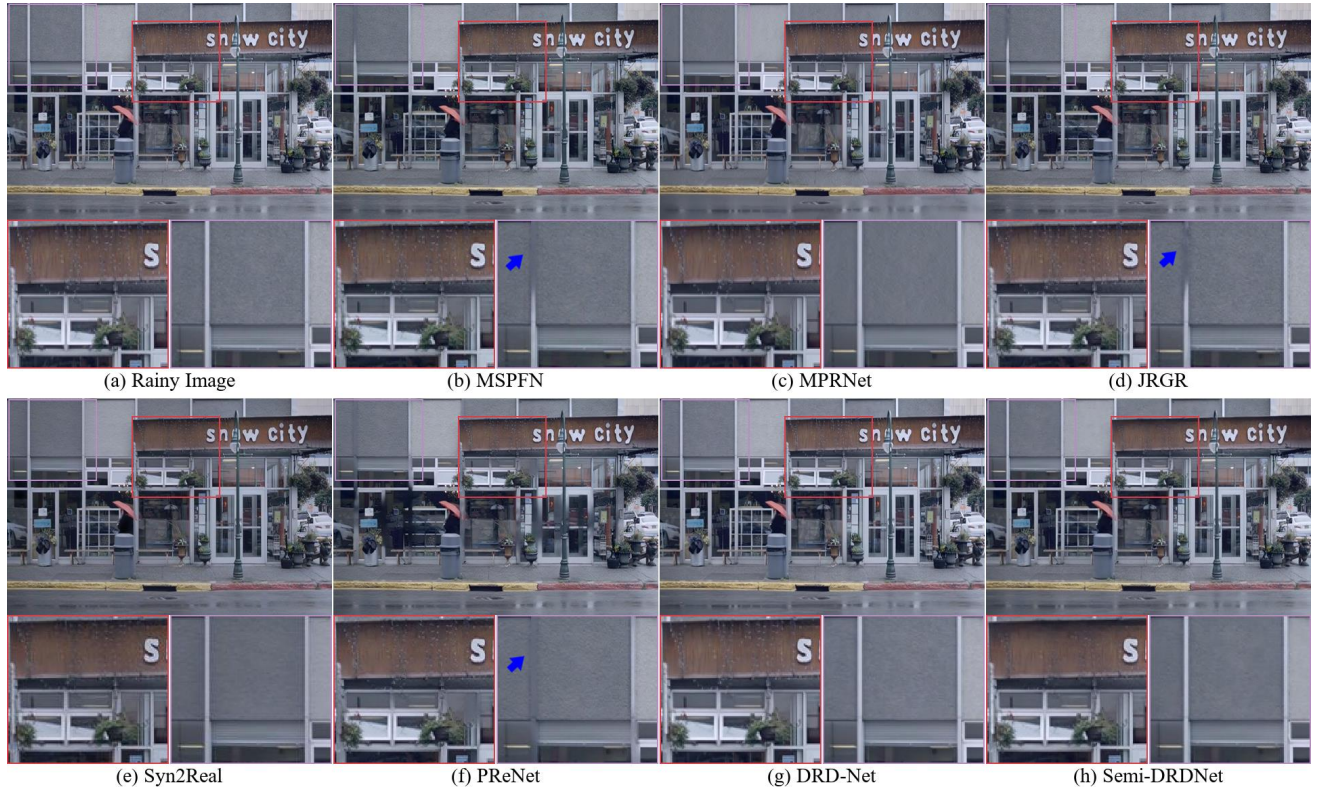


Fig. 8. Image deraining results tested in Real200. From (a)-(h): (a) the rainy image, and the deraining results of (b) MSPFN [2], (c) MPRNet [1], (d) JRGR [27], (e) Syn2Real [3], (f) PReNet [55], (g) our DRD-Net [4] and (h) our Semi-DRDNet. Meanwhile, MSPFN, JRGR and PReNet falsely remove some details, as denoted by blue arrow. Comparatively, our method can well handle the rain streaks while preserving texture details.

(the worst) to 10 (the best): 37 females and 63 males, aged 16 to 30 with a mean of 25.5. (3) We present rainy images and derained

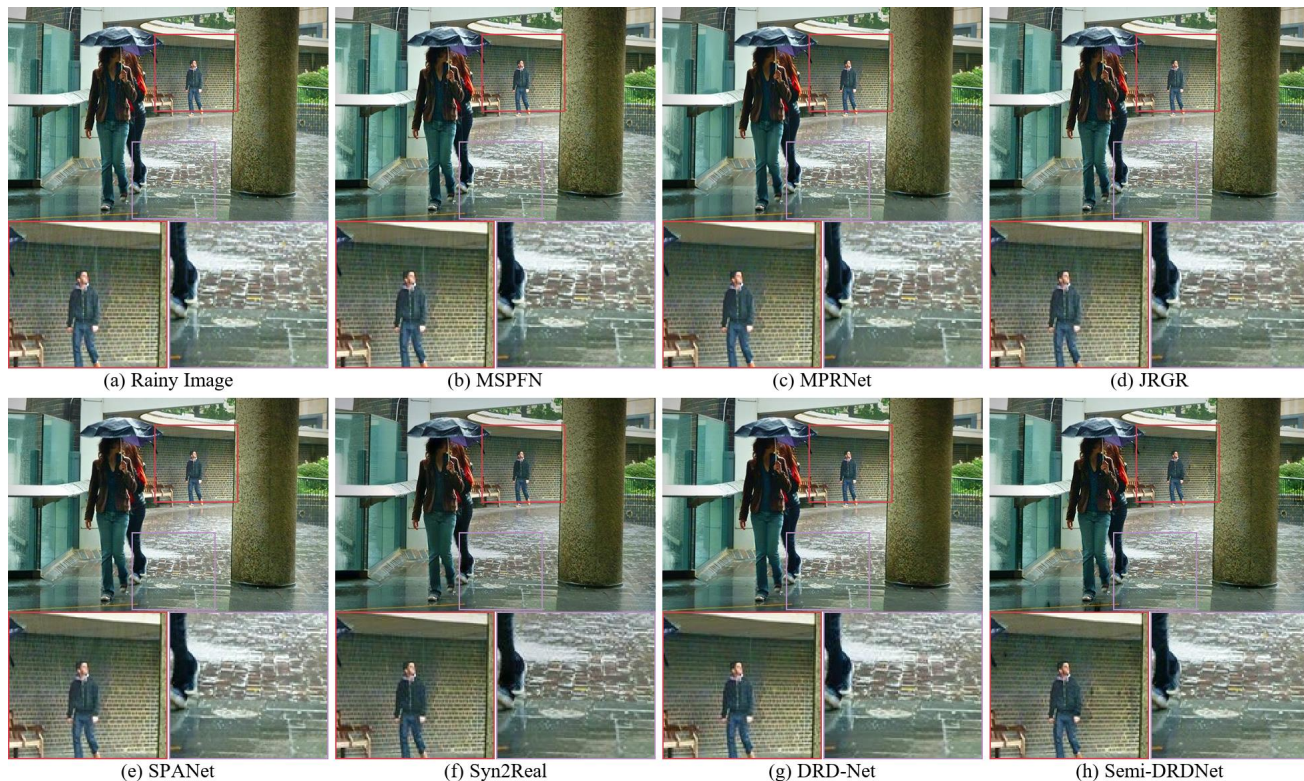


Fig. 9. Image deraining results tested in Real200. From (a)-(h): (a) the rainy image, and the deraining results of (b) MSPFN [2], (c) MPRNet [1], (d) JRGR [27], (e) SPA-Net [54], (f) Syn2Real [3], (g) our DRD-Net [4] and (h) our Semi-DRDNet.

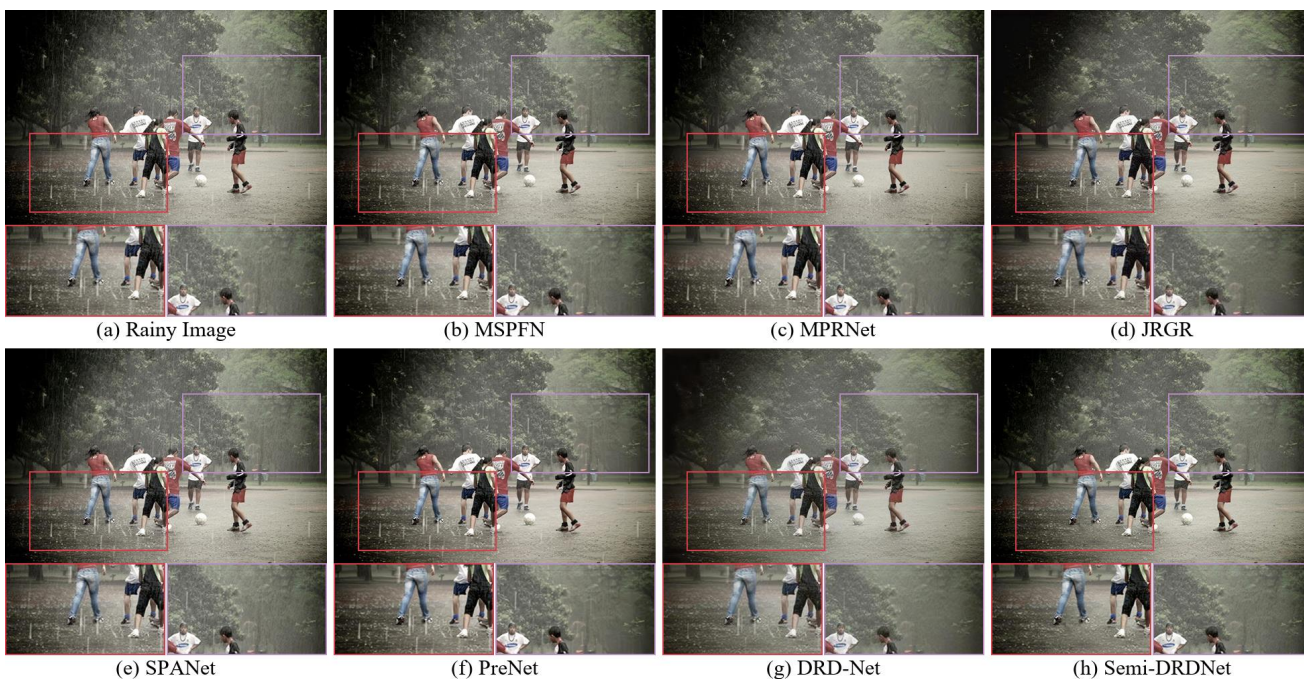


Fig. 10. Image deraining results tested in Real200. From (a)-(h): (a) the rainy image, and the deraining results of (b) MSPFN [2], (c) MPRNet [1], (d) JRGR [27], (e) SPA-Net [54], (f) PreNet [55], (g) our DRD-Net [4] and (h) our Semi-DRDNet.

images to each volunteer in a random order, and do not tell them which approach the derained image is generated by, then ask each of them to rate how the quality of the derained image is on a scale from 1 to 10. (4) We obtain 5000 ratings (100 volunteers \times 50 images per category) altogether per category: our Semi-DRDNet

and the other approaches. Fig. 15 reports the results, showing that our Semi-DRDNet has more pleasing derained images than the others. At the end of the user study, some participants report that for the majority of our derained images, they see no water splashing on the ground like the clean photos.



Fig. 11. Image deraining results tested in Real200. From (a)-(h): (a) the rainy image, and the deraining results of (b) MSPFN [2], (c) MPRNet [1], (d) JRGR [27], (e) SPA-Net [54], (f) Syn2Real [3], (g) our DRD-Net [4] and (h) our Semi-DRDNet.

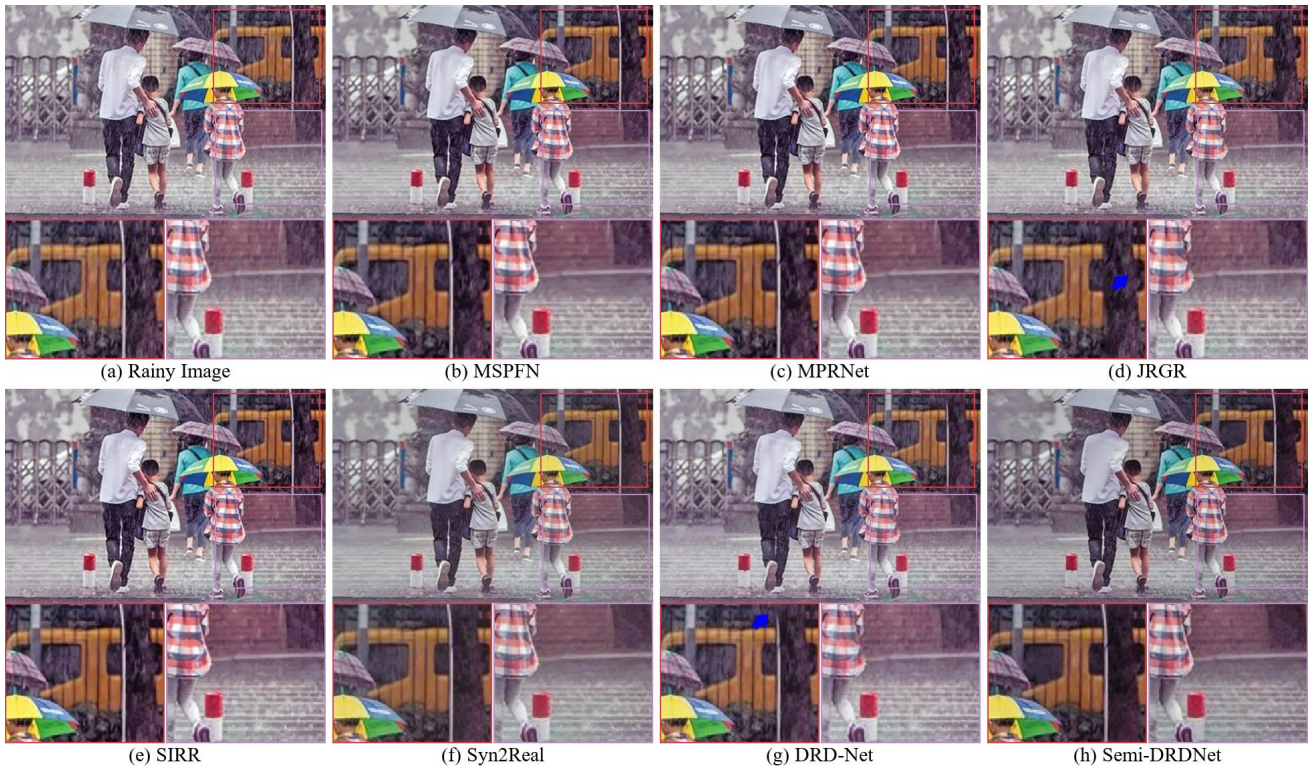


Fig. 12. Image deraining results tested in Real200. From (a)-(h): (a) the rainy image, and the deraining results of (b) MSPFN [2], (c) MPRNet [1], (d) JRGR [27], (e) SIRR [28], (f) Syn2Real [3], (g) our DRD-Net [4] and (h) our Semi-DRDNet.

4.4 Ablation Study

We conduct ablation experiments to gain insight into the respective roles of different components and loss functions. For

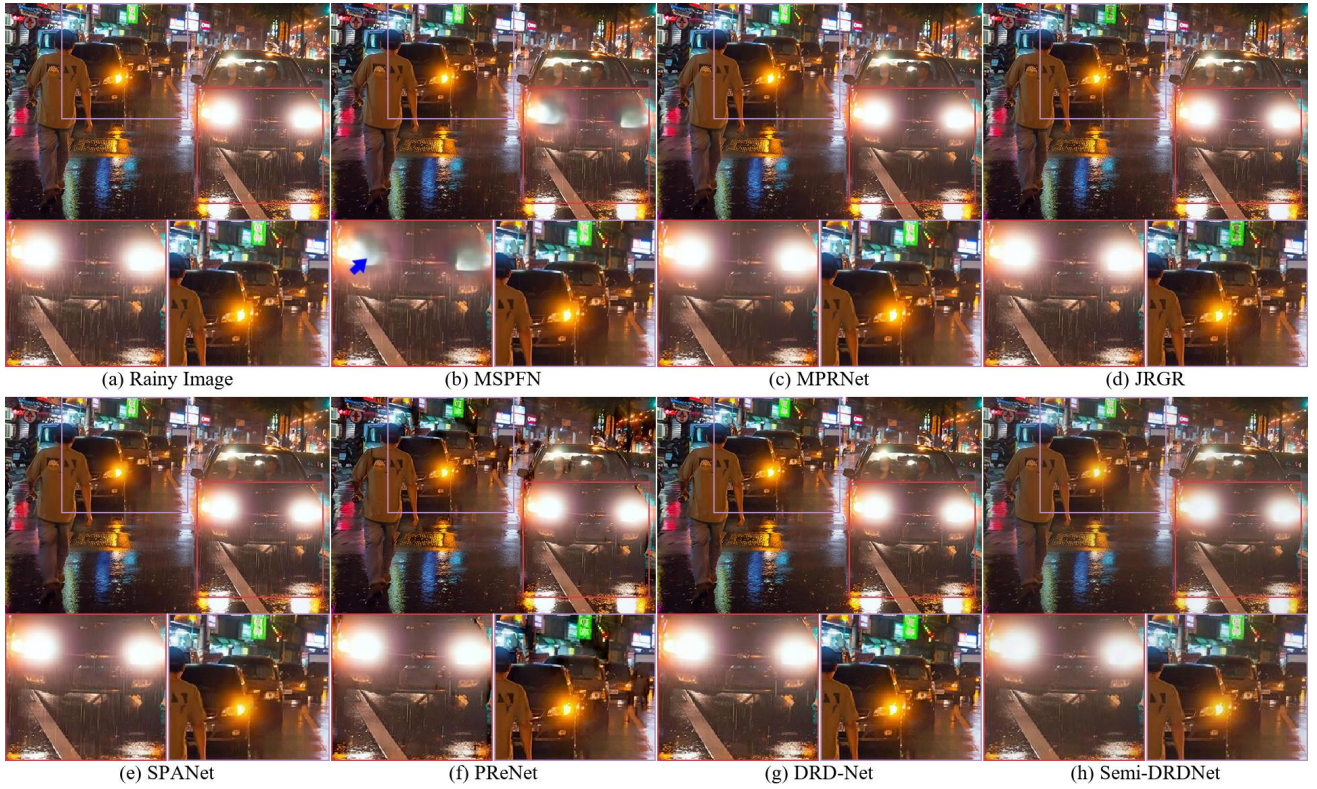


Fig. 13. Image deraining results tested in Real200. From (a)-(h): (a) the rainy image, and the deraining results of (b) MSPFN [2], (c) MPRNet [1], (d) JRGR [27], (e) SPA-Net [54], (f) PReNet [55], (g) our DRD-Net [4] and (h) our Semi-DRDNet.

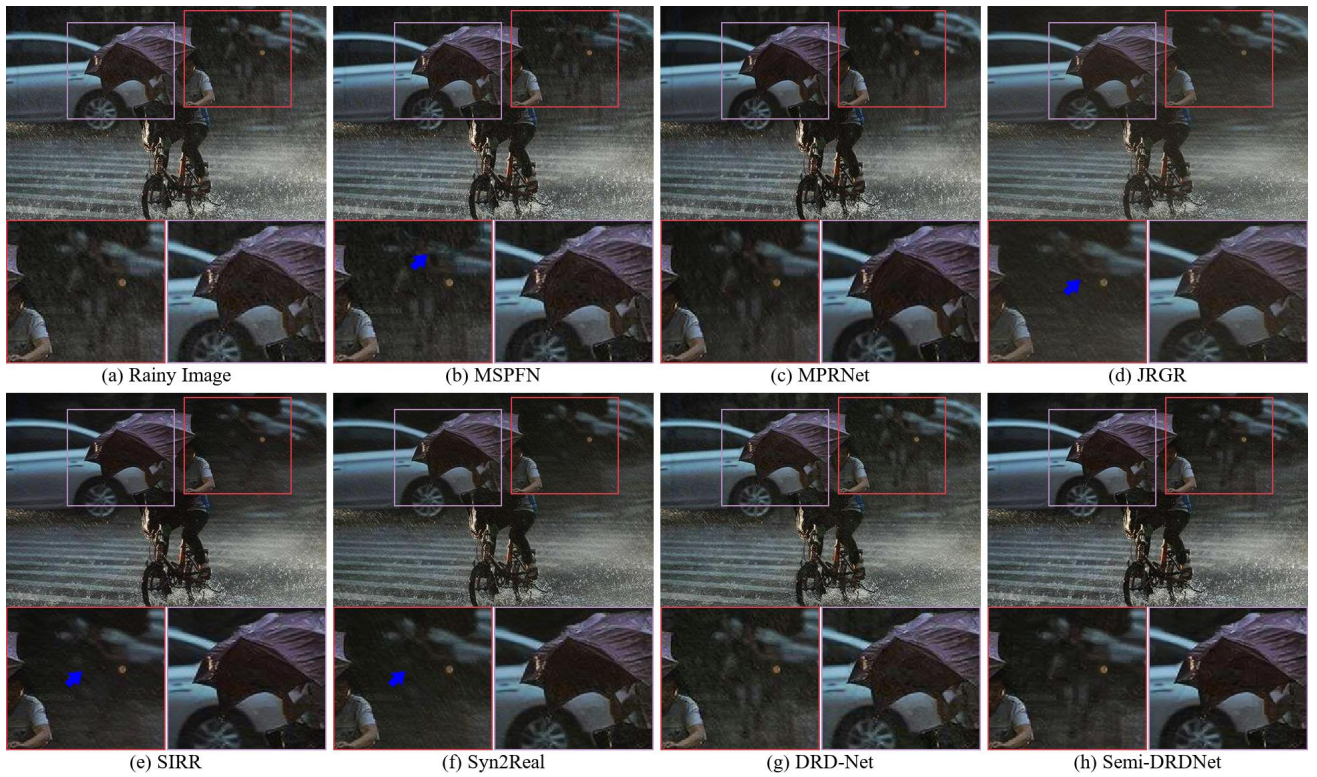


Fig. 14. Image deraining results tested in Real200. From (a)-(h): (a) the rainy image, and the deraining results of (b) MSPFN [2], (c) MPRNet [1], (d) JRGR [27], (e) SIRR [28], (f) Syn2Real [3], (g) our DRD-Net [4] and (h) our Semi-DRDNet.

fair comparisons, all models are trained on Rain200H&Real200, Rain200L&Real200, and Rain800&Real200.

Ablation Study on Different Components: To explore the effectiveness of our Semi-DRDNet, it is necessary to decompose

TABLE 2

Quantitative comparison between our Semi-DRDNet and other network architectures on the testing sets of Rain200L, Rain200H and Rain800. It is noteworthy that all models are trained in Rain200H&Real200, Rain200L&Real200, and Rain800&Real200.

Dataset	Metrics	BL	BL+SE	BL+SE+DB	BL+SE+RB	BL+SE+SDCAB	Semi-DRDNet
Rain200L	PSNR	35.69	36.25	36.93	37.16	37.24	37.82
	SSIM	0.9782	0.9796	0.9804	0.9876	0.9879	0.9884
Rain200H	PSNR	26.33	26.79	27.45	27.32	28.32	28.68
	SSIM	0.8323	0.8441	0.9194	0.9086	0.9221	0.9236
Rain800	PSNR	25.94	26.35	26.39	26.45	26.56	26.74
	SSIM	0.8132	0.8217	0.8945	0.8978	0.9024	0.9042

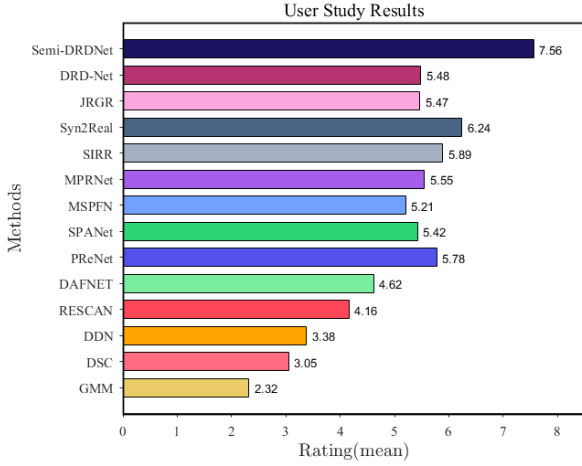


Fig. 15. User study results. Mean ratings (from 1 (bad) to 10 (good)) given by the participants on the Rain200H&Real200 dataset.

its full scheme into different parts and even replace the network architecture for the ablation study.

- **BL:** Baseline (BL) indicates the residual network without the SE operation, which learns a function that maps the rainy images to the rain streaks.
- **BL+SE:** Adding the SE operation to the baseline.
- **BL+SE+DB:** Employing two sub-networks for image deraining. One network is the rain residual network (BL+SE), and the another is detail repair network based on the direct block (DB, see in Fig. 5(a)).
- **BL+SE+RB:** DB is replaced with residual block (RB) in the detail repair network.
- **BL+SE+SDCAB:** Comprising the rain residual network (BL+SE) and the detail repair network based on the proposed structure detail context aggregation block (SDCAB). Although this model has the same network structure as DRD-Net [4] (our conference version), it trains in a semi-supervised manner with different loss functions.
- **BL+SE+SDCAB+UCR:** Semi-DRDNet comprises the rain residual network (BL+SE), the detail repair network based on the proposed structure detail context aggregation block (SDCAB), and the unpaired contrastive regularization network (UCR) with the unpaired contrastive loss.

Effect of SE, SDCAB and UCR: To validate the necessity of the structure in Figs. 2 and 5, we show the results in Table 2 and Figs. 16-17. It is found that: (i) The performance of deraining without the SE operation suffers from slight degradation. This certifies the necessity of the SE operation from another side. (ii)

TABLE 3

Ablation study on different settings of our method in Rain200H. M denotes the number of feature maps in our network and D is the total depth of our network.

	Metrics	M = 16	M = 32	M = 64
D = 8+3	PSNR	26.42	26.82	26.99
	SSIM	0.9102	0.9124	0.9142
D = 12+3	PSNR	26.58	26.90	27.38
	SSIM	0.9104	0.9134	0.9161
D = 16+3	PSNR	26.97	27.68	28.68
	SSIM	0.9138	0.9190	0.9236

TABLE 4

Ablation study on different loss functions of our method in Rain200L, and w/o denotes without.

Setting	w/o	0.1	0.5	1.0
L_{tv}	37.53/0.9874	37.82/0.9884	37.66/0.9879	37.23/0.9817
L_{ide}	37.06/0.9835	37.21/0.9844	37.82/0.9884	37.35/0.9839
L_{per}	36.98/0.9822	37.02/0.9826	37.82/0.9884	37.08/0.9831
L_r	36.78/0.9794	37.82/0.9884	37.46/0.9864	37.78/0.9880
L_{ucr}	-	36.56/0.9782	37.82/0.9884	37.58/0.9858

The performance of deraining without the detail recovery network suffers from image detail blurring in the real-world images (Figs. 16), which proves the necessity of DRN to find the lost details. (iii) In order to evaluate the effectiveness of SDCAB, we compare our network with other connection style blocks, including the direct block (DB), the residual block (RB) which has been used in DDN [10]. For fair comparisons, we replace SDCAB with DB and RB respectively, the result (shown in Table 2) certifies that SDCAB is essential to detail-recovery image deraining. (iv) Moreover, the full scheme of BL+SE+SDCAB+UCR outperforms other architectures both quantitatively and qualitatively, which certifies that UCR can constrain the deraining network to approximate the clean images and move away from the real rainy images, thus benefiting real-world rain removal.

Effect of Parameter Settings: Results under different parameter settings of Semi-DRDNet can be found in Table 3. We have discussed the effects of the number of feature maps and SDCAB or the rain residual blocks (RRB). The table shows that more parameters lead to higher performance.

Effect of Loss Functions: We evaluate the deraining performance by considering different combinations of loss functions (see Table 4 and Fig. 17) which demonstrate that: 1) The introduction of the rain residual loss has greatly improved the performance of the model. 2) The hybrid loss in our semi-supervised paradigm can optimize our network effectively. Especially, the unsupervised loss functions such as the TV loss, identity loss, perceptual loss



Fig. 16. Qualitative comparison between our Semi-DRDNet and other network architectures in Real200. From (a)-(g): (a) the real-world rainy image, and the deraining results of (b) BL, (c) BL+SE, (d) BL+SE+DB, (e) BL+SE+RB, (f) BL+SE+SDCAB, (g) without tv loss and (h) the full scheme of Semi-DRDNet, respectively. All models are trained on Rain200L&Real200, and tested in Real200.

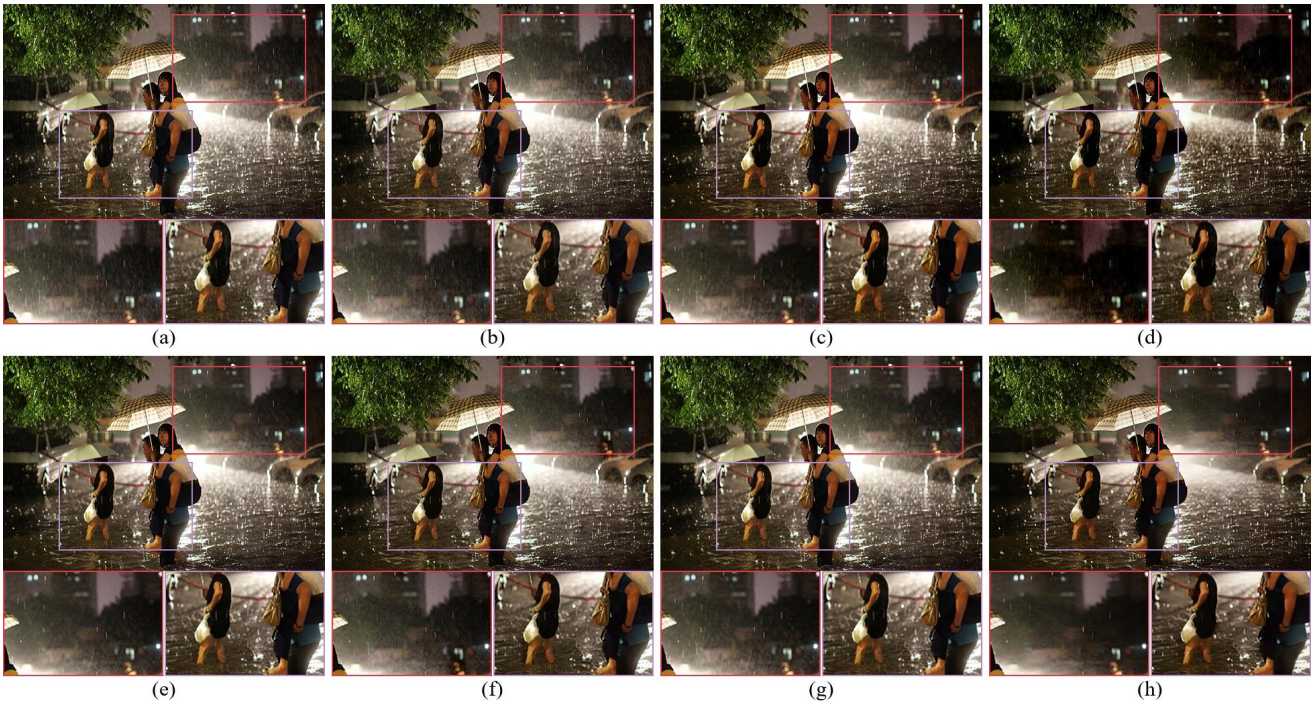


Fig. 17. Qualitative comparison between our Semi-DRDNet and other network architectures in Real200. From (a)-(g): (a) the real-world rainy images, and the deraining results of (b) BL+SE, (c) BL+SE+SDCAB, (d) without perceptual loss, (e) without identity loss, (f) without tv loss, (g) without rain residual loss and (h) the full scheme of Semi-DRDNet, respectively. All models are trained on Rain200L&Real200, and tested in Real200.

and unpaired contrastive loss can constrain the model to generate more realistic images.

4.5 Analysis of DRN

Existing learning-based deraining methods resort to delicate network design to meet the challenging goal of removing rain streaks

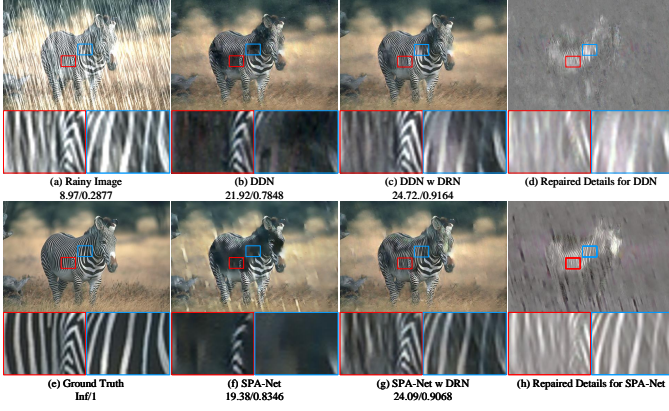


Fig. 18. Image deraining performance in Rain200H. From (a)-(h): (a) the rainy image Zebra, the deraining results of (b) DDN [10], (c) DDN with Detail Repair Network, (f) SPA-Net [54], (g) SPA-Net with Detail Repair Network, (d) and (h) are the repaired details of DDN and SPA-Net, and (e) the ground-truth image.



Fig. 19. Image deraining performance in Rain200H. From (a)-(h): (a) the rainy image Car, the deraining results of (b) DDN [10], (c) DDN with Detail Repair Network, (f) SPA-Net [54], (g) SPA-Net with Detail Repair Network, (d) and (h) are the repaired details of DDN and SPA-Net, and (e) the ground-truth image.

but retaining details of similar properties. In contrast, our Semi-DRDNet decomposes this conflicting task into ‘remove’ and ‘repair’ by two parallel network branches, which share the same input and collaborate to spit a high-fidelity output. Apparently, the choice of the rain removal part is not unique, the detail recovery branch can be easily attached to existing deraining networks to boost their performance.

Detail Recovery for Synthetic Images. Taking DDN [10] and SPA [54] as examples, we experiment with two parallel networks consisting of our detail repair network and their deraining networks. For fair comparisons, we keep most parameters from the

TABLE 5
Quantitative evaluation, DDN w/ DRN indicates DDN incorporated with the detail repair network.

Datasets	Metrics	DDN	DDN w/ DRN	SPA	SPA w/ DRN
Rain200H	PSNR	24.64	25.92	23.04	25.68
	Time	0.03s	0.15s	0.06s	0.45s
Rain800	PSNR	24.04	25.13	22.41	25.67
	Time	0.05s	0.14s	0.26s	0.35s

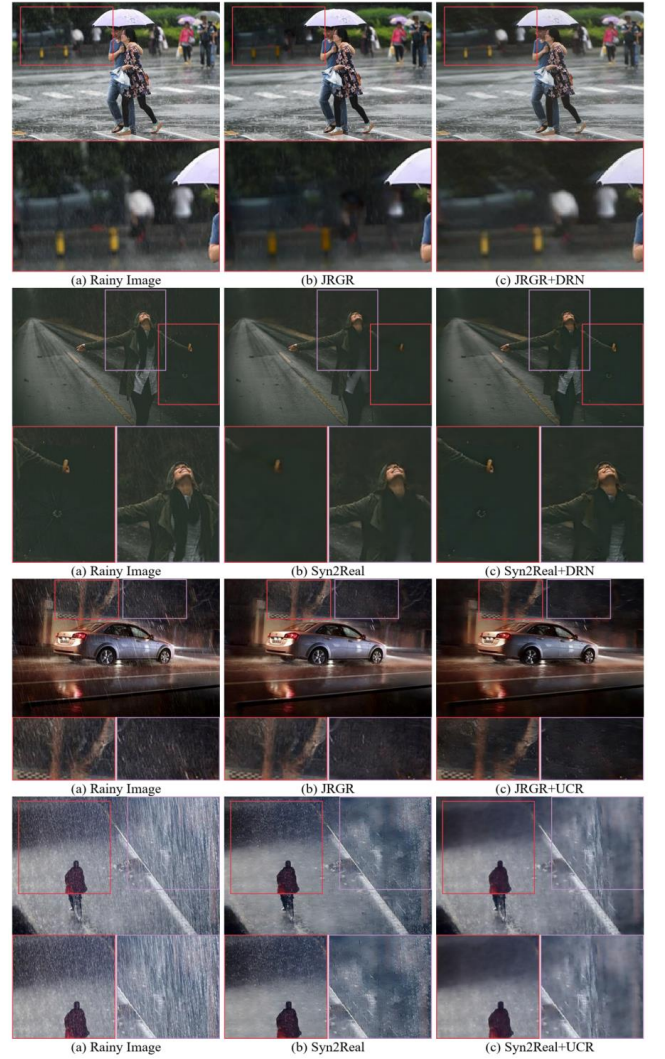


Fig. 20. Image deraining results tested in Real200. Note that all models are trained on Rain200H&Real200. It is noteworthy that JRGR includes four deraining sub-networks, thus we add four additional parallel DRNs and cascaded UCRs to these sub-networks for the joint training of JRGR.

original DDN and SPA untouched. The depth and the number of feature channels of the detail repair network are set as 24 and 16 respectively. We randomly select 20 image patches with the size of 64×64 to train the networks. We compare PSNR and the running time of deraining methods with and without our detail recovery mechanism on different datasets. From Table 5 we observe that attaching our detail repair network considerably improves PSNR while sacrificing negligible time efficiency. In this section, visual results are provided for a better understanding on the effectiveness of the proposed detail recovery mechanism. Figs. 18 and 19 show that deraining networks tend to lose details which share similar properties with rain streaks, such as the zebra-stripe in Fig. 18 and the fishing rod in Fig. 19. We demonstrate that by simply incorporating our detail repair network, these lost details can be easily added back to restore the high-quality rain-free images.

Detail Recovery for Real-world Images. To our knowledge, recent semi-supervised deraining paradigms have paid little attention to detail recovery yet. To certify that the detail recovery is also essential to real-world image deraining, we incorporate

DRN into the semi-supervised deraining paradigms [27] and [3]. It is noteworthy that JRGR includes four deraining sub-networks, thus we add four additional parallel DRNs to these sub-networks for the joint training of JRGR. From Fig. 20 we can observe that DRN can also effectively find back the lost details during the semi-supervised deraining process, and obtain better deraining performance on real-world images. Thus, it is reasonable to view rain removal and detail recovery as two separate tasks, so that each part could be specialized rather than traded off.

TABLE 6
Quantitative evaluation, SDCAB and MSARR indicate DRN based on SDCAB and MSARR, respectively.

Datasets	Metrics	SDCAB	MSARR
Rain200H	PSNR	28.68	26.78
	Time	0.48s	0.42s
Rain800	PSNR	26.74	25.39
	Time	0.64s	0.58s

SDCAB vs MSARR. We train our detail repair network based on MSARR and observe that the performance drops from 28.68 dB to 26.78 dB on the testing set of Rain200H (see Table 6), compared to DRN based on SDCAB. This shows that SDCAB can be used for designing a better detail recovery branch. The detailed structure of the detail repair network is presented in Table 7, illustrating how the receptive field grows by applying the SDCAB block with multi-scale dilations.

4.6 Analysis of UCR

Existing semi-supervised deraining approaches tend to adopt the clean images as positive samples to guide the semi-supervised paradigm but neglect to utilize the rainy images as negative samples. In contrast, an unpaired contrastive regularization network is designed to learn useful information from both clean and rainy images. To verify the effectiveness of UCR for real-world image deraining, we also incorporate UCR into the semi-supervised deraining method [27] and [3]. Fig. 20 shows that the prevalent semi-supervised paradigms may fail on heavy real rainy images due to the lack of supervision for unpaired data. Meanwhile, our UCR can make full use of unpaired positives (clean images)/negatives (rainy images), enabling them to obtain better results even with heavy rain.

4.7 Running Time

We compare the running time of our method with different approaches on the dataset of Rain200H&Real200 in Fig. 21. It is observed that our method is not the fastest one, but its performance is still acceptable.

4.8 Application

To demonstrate that our Semi-DRDNet can benefit vision-based applications, we employ Google Vision API to evaluate the deraining results. One of the results is shown in Fig. 22 (a-b). It is observed that the Google API can recognize the rainy weather in the rainy image while it cannot recognize the rainy weather in the derained image. Furthermore, we use the Google API to test 100 sets of the real-world rainy images and derained images of our Semi-DRDNet, DRD-Net [4] and three semi-supervised methods [3], [27], [28] in Fig. 22 (c). After deraining, the confidences in recognizing rain from the images are significantly reduced.

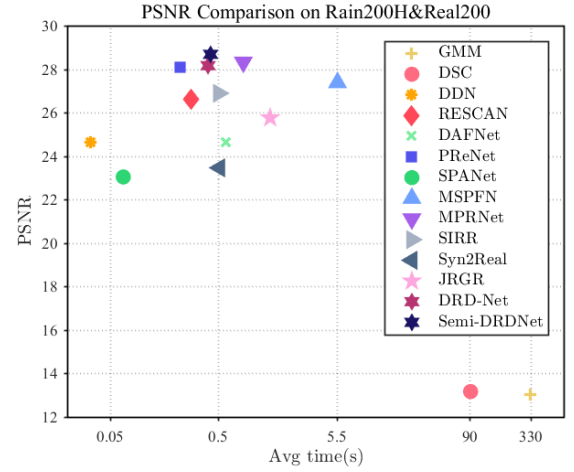


Fig. 21. Averaged time and performance of different methods.

5 CONCLUSION

In this paper, we respond to the question and obtain the answer that leveraging both accessible unpaired clean/rainy yet real-world images and additional detail repair guidance, can improve the generalization ability of a deraining model. We propose a semi-supervised detail-recovery image deraining network (Semi-DRDNet). Semi-DRDNet consists of three sub-networks for deraining real-world rainy images. First, a rain residual network is designed to remove the rain streaks from the rainy images. Second, an additional detail repair network is proposed to find back the details to the derained images. Third, a novel unpaired contrastive regularization network is developed to supervise with the unlabeled samples, thus enhancing the real-world image deraining ability. Qualitative and quantitative experiments indicate that our method outperforms the state-of-the-art supervised and semi-supervised approaches in terms of removing the rain streaks and recovering the image details.

REFERENCES

- [1] S. W. Zamir, A. Arora, S. Khan, M. Hayat, F. S. Khan, M.-H. Yang, and L. Shao, "Multi-stage progressive image restoration," in *Proceedings of the IEEE/CVF Conference on Computer Vision and Pattern Recognition*, 2021, pp. 14 821–14 831.
- [2] K. Jiang, Z. Wang, P. Yi, C. Chen, B. Huang, Y. Luo, J. Ma, and J. Jiang, "Multi-scale progressive fusion network for single image deraining," in *Proceedings of the IEEE/CVF conference on computer vision and pattern recognition*, 2020, pp. 8346–8355.
- [3] R. Yasarla, V. A. Sindagi, and V. M. Patel, "Syn2real transfer learning for image deraining using gaussian processes," in *Proceedings of the IEEE/CVF conference on computer vision and pattern recognition*, 2020, pp. 2726–2736.
- [4] S. Deng, M. Wei, J. Wang, Y. Feng, L. Liang, H. Xie, F. L. Wang, and M. Wang, "Detail-recovery image deraining via context aggregation networks," in *Proceedings of the IEEE/CVF conference on computer vision and pattern recognition*, 2020, pp. 14 560–14 569.
- [5] Y. Li, R. T. Tan, X. Guo, J. Lu, and M. S. Brown, "Rain streak removal using layer priors," in *2016 IEEE Conference on Computer Vision and Pattern Recognition*, vol. 12, 2016, pp. 2736–2744.
- [6] Y. Luo, Y. Xu, and H. Ji, "Removing rain from a single image via discriminative sparse coding," in *2015 IEEE International Conference on Computer Vision*, vol. 8, 2015, pp. 3397–3405.
- [7] L.-W. Kang, C.-W. Lin, and Y.-H. Fu, "Automatic single-image-based rain streaks removal via image decomposition," *IEEE Transactions on Image Processing*, vol. 21, no. 4, pp. 1742–1755, 2011.
- [8] H. Zhang and V. M. Patel, "Convolutional sparse and low-rank coding-based rain streak removal," in *2017 IEEE Winter Conference on Applications of Computer Vision*, 2017, pp. 1259–1267.

TABLE 7
The detailed architecture of the detail repair network.

Layer	0	1	2	...	d	...	16	17	18
Convolution	3×3	3×3	3×3	...	3×3	...	3×3	3×3	3×3
SDCAB	No	Yes	Yes	...	Yes	...	Yes	No	No
Dilation	1	7	7	...	7	...	7	1	1
Receptive field	3×3	17×17	31×31	...	$(d-1) \times 14 + 17$...	227×227	229×229	231×231

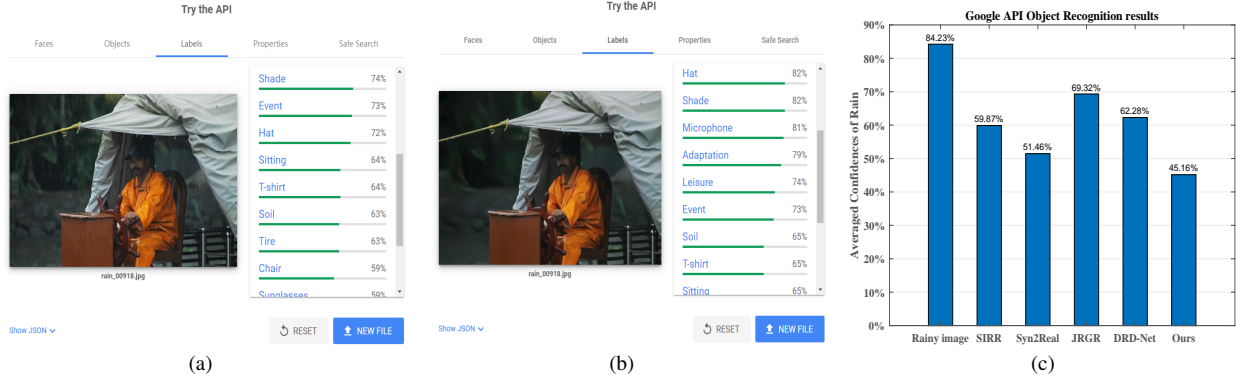


Fig. 22. The deraining results tested on the Google Vision API. From (a)-(c): (a) the object recognition result in the real-world rainy image, (b) the object recognition result after deraining by our Semi-DRDNet, and (c) the averaged confidences in recognizing rain from 100 sets of the real-world rainy images and derained images of SIRR [28], Syn2Real [3], JRGR [27], DRD-Net [4] and our Semi-DRDNet respectively. Note: zero confidence refers to a total failure in recognizing rain from a derained image by the Google API.

- [9] X. Guo, X. Xie, G. Liu, M. Wei, and J. Wang, "Robust low-rank subspace segmentation with finite mixture noise," *Pattern Recognition*, vol. 93, pp. 55–67, 2019.
- [10] X. Fu, J. Huang, D. Zeng, Y. Huang, X. Ding, and J. W. Paisley, "Removing rain from single images via a deep detail network," in *2017 IEEE Conference on Computer Vision and Pattern Recognition*, 2017, pp. 1715–1723.
- [11] Y. Wang, C. Ma, and B. Zeng, "Multi-decoding deraining network and quasi-sparsity based training," in *Proceedings of the IEEE/CVF Conference on Computer Vision and Pattern Recognition*, 2021, pp. 13 375–13 384.
- [12] W. Yang, R. T. Tan, J. Feng, S. Wang, B. Cheng, and J. Liu, "Recurrent multi-frame deraining: Combining physics guidance and adversarial learning," *IEEE Transactions on Pattern Analysis and Machine Intelligence*, 2021.
- [13] W. Yang, R. T. Tan, J. Feng, Z. Guo, S. Yan, and J. Liu, "Joint rain detection and removal from a single image with contextualized deep networks," *IEEE transactions on pattern analysis and machine intelligence*, vol. 42, no. 6, pp. 1377–1393, 2019.
- [14] R. Quan, X. Yu, Y. Liang, and Y. Yang, "Removing raindrops and rain streaks in one go," in *Proceedings of the IEEE/CVF Conference on Computer Vision and Pattern Recognition*, 2021, pp. 9147–9156.
- [15] Y. Wang, Y. Song, C. Ma, and B. Zeng, "Rethinking image deraining via rain streaks and vapors," in *European Conference on Computer Vision*, 2020, pp. 367–382.
- [16] H. Zhang, V. Sindagi, and V. M. Patel, "Image de-raining using a conditional generative adversarial network," *IEEE transactions on circuits and systems for video technology*, vol. 30, no. 11, pp. 3943–3956, 2019.
- [17] X. Fu, Q. Qi, Z.-J. Zha, Y. Zhu, and X. Ding, "Rain streak removal via dual graph convolutional network," in *Proc. AAAI Conf. Artif. Intell.*, 2021, pp. 1–9.
- [18] X. Li, J. Wu, Z. Lin, H. Liu, and H. Zha, "Recurrent squeeze-and-excitation context aggregation net for single image deraining," in *Computer Vision - ECCV 2018 - 15th European Conference, Munich, Germany, September 8-14, 2018, Proceedings, Part VII*, 2018, pp. 262–277.
- [19] H. Chen, Y. Wang, T. Guo, C. Xu, Y. Deng, Z. Liu, S. Ma, C. Xu, C. Xu, and W. Gao, "Pre-trained image processing transformer," in *Proceedings of the IEEE/CVF Conference on Computer Vision and Pattern Recognition*, 2021, pp. 12 299–12 310.
- [20] Z. Fan, H. Wu, X. Fu, Y. Huang, and X. Ding, "Residual-guide network for single image deraining," in *2018 ACM Multimedia Conference on Multimedia Conference*, 2018, pp. 1751–1759.
- [21] X. Liu, M. Suganuma, Z. Sun, and T. Okatani, "Dual residual networks leveraging the potential of paired operations for image restoration," in *Proceedings of the IEEE Conference on Computer Vision and Pattern Recognition*, 2019, pp. 7007–7016.
- [22] C. Chen and H. Li, "Robust representation learning with feedback for single image deraining," in *Proceedings of the IEEE/CVF Conference on Computer Vision and Pattern Recognition*, 2021, pp. 7742–7751.
- [23] R. Li, L.-F. Cheong, and R. T. Tan, "Heavy rain image restoration: Integrating physics model and conditional adversarial learning," in *Proceedings of the IEEE Conference on Computer Vision and Pattern Recognition*, 2019, pp. 1633–1642.
- [24] D. Ren, W. Zuo, D. Zhang, L. Zhang, and M.-H. Yang, "Simultaneous fidelity and regularization learning for image restoration," *IEEE transactions on pattern analysis and machine intelligence*, vol. 43, no. 1, pp. 284–299, 2019.
- [25] G. Wang, C. Sun, and A. Sowmya, "Erl-net: Entangled representation learning for single image de-raining," in *Proceedings of the IEEE International Conference on Computer Vision*, 2019, pp. 5644–5652.
- [26] J. Xiao, M. Zhou, X. Fu, A. Liu, and Z.-J. Zha, "Improving de-raining generalization via neural reorganization," in *Proceedings of the IEEE/CVF International Conference on Computer Vision*, 2021, pp. 4987–4996.
- [27] Y. Ye, Y. Chang, H. Zhou, and L. Yan, "Closing the loop: Joint rain generation and removal via disentangled image translation," in *Proceedings of the IEEE/CVF Conference on Computer Vision and Pattern Recognition*, 2021, pp. 2053–2062.
- [28] W. Wei, D. Meng, Q. Zhao, Z. Xu, and Y. Wu, "Semi-supervised transfer learning for image rain removal," in *Proceedings of the IEEE Conference on Computer Vision and Pattern Recognition*, 2019, pp. 3877–3886.
- [29] W. Yang, R. T. Tan, J. Feng, J. Liu, Z. Guo, and S. Yan, "Deep joint rain detection and removal from a single image," in *Proceedings of the IEEE Conference on Computer Vision and Pattern Recognition*, 2017, pp. 1357–1366.
- [30] Q. Wu, L. Wang, K. N. Ngan, H. Li, and F. Meng, "Beyond synthetic data: A blind deraining quality assessment metric towards authentic rain image," in *2019 IEEE International Conference on Image Processing (ICIP)*, 2019, pp. 2364–2368.
- [31] S. Li, I. B. Araujo, W. Ren, Z. Wang, E. K. Tokuda, R. H. Junior, R. Cesar-Junior, J. Zhang, X. Guo, and X. Cao, "Single image deraining: A comprehensive benchmark analysis," in *Proceedings of the IEEE/CVF Conference on Computer Vision and Pattern Recognition*, 2019, pp. 3838–3847.
- [32] Z. Wu, Y. Xiong, S. X. Yu, and D. Lin, "Unsupervised feature learning via non-parametric instance discrimination," in *Proceedings of the IEEE*

- conference on computer vision and pattern recognition, 2018, pp. 3733–3742.
- [33] K. He, H. Fan, Y. Wu, S. Xie, and R. Girshick, “Momentum contrast for unsupervised visual representation learning,” in *Proceedings of the IEEE/CVF Conference on Computer Vision and Pattern Recognition*, 2020, pp. 9729–9738.
- [34] T. Chen, S. Kornblith, M. Norouzi, and G. Hinton, “A simple framework for contrastive learning of visual representations,” in *International conference on machine learning*, 2020, pp. 1597–1607.
- [35] N. Saunshi, O. Plevrakis, S. Arora, M. Khodak, and H. Khandeparkar, “A theoretical analysis of contrastive unsupervised representation learning,” in *International Conference on Machine Learning*, 2019, pp. 5628–5637.
- [36] H. Wu, Y. Qu, S. Lin, J. Zhou, R. Qiao, Z. Zhang, Y. Xie, and L. Ma, “Contrastive learning for compact single image dehazing,” in *Proceedings of the IEEE/CVF Conference on Computer Vision and Pattern Recognition*, 2021, pp. 10 551–10 560.
- [37] D. Liang, L. Li, M. Wei, S. Yang, L. Zhang, W. Yang, Y. Du, and H. Zhou, “Semantically contrastive learning for low-light image enhancement,” *CoRR*, vol. abs/1609.07769, 2021.
- [38] K. Zhang, W. Zuo, Y. Chen, D. Meng, and L. Zhang, “Beyond a gaussian denoiser: Residual learning of deep cnn for image denoising,” *IEEE Transactions on Image Processing*, vol. 26, no. 7, pp. 3142–3155, 2017.
- [39] J. Hu, L. Shen, and G. Sun, “Squeeze-and-excitation networks,” in *2018 IEEE Conference on Computer Vision and Pattern Recognition*, 2018, pp. 7132–7141.
- [40] G. Li, X. He, W. Zhang, H. Chang, L. Dong, and L. Lin, “Non-locally enhanced encoder-decoder network for single image de-raining,” in *Proceedings of the 26th ACM international conference on Multimedia*, 2018, pp. 1056–1064.
- [41] D.-A. Huang, L.-W. Kang, M.-C. Yang, C.-W. Lin, and Y.-C. F. Wang, “Context-aware single image rain removal,” in *2012 IEEE International Conference on Multimedia and Expo*. IEEE, 2012, pp. 164–169.
- [42] W. Yang, R. T. Tan, J. Feng, J. Liu, Z. Guo, and S. Yan, “Joint rain detection and removal via iterative region dependent multi-task learning,” *CoRR*, vol. abs/1609.07769, 2016.
- [43] W. Li, X. Yang, M. Kong, L. Wang, J. Huo, Y. Gao, and J. Luo, “Triplet is all you need with random mappings for unsupervised visual representation learning,” *arXiv preprint arXiv:2107.10419*, 2021.
- [44] H. A. Aly and E. Dubois, “Image up-sampling using total-variation regularization with a new observation model,” *IEEE Transactions on Image Processing*, vol. 14, no. 10, pp. 1647–1659, 2005.
- [45] J.-Y. Zhu, T. Park, P. Isola, and A. A. Efros, “Unpaired image-to-image translation using cycle-consistent adversarial networks,” in *Proceedings of the IEEE international conference on computer vision*, 2017, pp. 2223–2232.
- [46] J. Johnson, A. Alahi, and L. Fei-Fei, “Perceptual losses for real-time style transfer and super-resolution,” in *European conference on computer vision*, 2016, pp. 694–711.
- [47] W. Yang, R. T. Tan, J. Feng, J. Liu, Z. Guo, and S. Yan, “Deep joint rain detection and removal from a single image,” in *2017 IEEE Conference on Computer Vision and Pattern Recognition*, 2017, pp. 1685–1694.
- [48] H. Huang, A. Yu, and R. He, “Memory oriented transfer learning for semi-supervised image deraining,” in *Proceedings of the IEEE/CVF Conference on Computer Vision and Pattern Recognition*, 2021, pp. 7732–7741.
- [49] Y. Wei, Z. Zhang, Y. Wang, H. Zhang, M. Zhao, M. Xu, and M. Wang, “Semi-deraingan: A new semi-supervised single image deraining,” in *2021 IEEE International Conference on Multimedia and Expo (ICME)*. IEEE, 2021, pp. 1–6.
- [50] K. He, X. Zhang, S. Ren, and J. Sun, “Delving deep into rectifiers: Surpassing human-level performance on imagenet classification,” in *2015 IEEE International Conference on Computer Vision*, 2015, pp. 1026–1034.
- [51] D. P. Kingma and J. Ba, “Adam: A method for stochastic optimization,” *arXiv preprint arXiv:1412.6980*, 2014.
- [52] Y. Luo, Y. Xu, and H. Ji, “Removing rain from a single image via discriminative sparse coding,” in *2015 IEEE International Conference on Computer Vision*, 2015, pp. 3397–3405.
- [53] X. Hu, C.-W. Fu, L. Zhu, and P.-A. Heng, “Depth-attentional features for single-image rain removal,” in *The IEEE Conference on Computer Vision and Pattern Recognition (CVPR)*, 2019.
- [54] T. Wang, X. Yang, K. Xu, S. Chen, Q. Zhang, and R. W. Lau, “Spatial attentive single-image deraining with a high quality real rain dataset,” in *Proceedings of the IEEE Conference on Computer Vision and Pattern Recognition*, 2019, pp. 12 270–12 279.
- [55] D. Ren, W. Zuo, Q. Hu, P. Zhu, and D. Meng, “Progressive image deraining networks: a better and simpler baseline,” in *Proceedings of the IEEE Conference on Computer Vision and Pattern Recognition*, 2019, pp. 3937–3946.
- [56] Z. Wang, A. C. Bovik, H. R. Sheikh, and E. P. Simoncelli, “Image quality assessment: from error visibility to structural similarity,” *IEEE transactions on image processing*, vol. 13, no. 4, pp. 600–612, 2004.